

# **Crushing Strength of Aluminum Oxide Agglomerates**

R. A. Gamble  
Sverdrup Technology, Inc.

**July 1985**

Property of U. S. Air Force  
AEDC LIBRARY  
F40600-81-C-0004

**Final Report for Period April 1983 through September 1984**

**TECHNICAL REPORTS  
FILE COPY**

Approved for public release; distribution unlimited.

**ARNOLD ENGINEERING DEVELOPMENT CENTER  
ARNOLD AIR FORCE STATION, TENNESSEE  
AIR FORCE SYSTEMS COMMAND  
UNITED STATES AIR FORCE**

## NOTICES

When U. S. Government drawings, specifications, or other data are used for any purpose other than a definitely related Government procurement operation, the Government thereby incurs no responsibility nor any obligation whatsoever, and the fact that the government may have formulated, furnished, or in any way supplied the said drawings, specifications, or other data, is not to be regarded by implication or otherwise, or in any manner licensing the holder or any other person or corporation, or conveying any rights or permission to manufacture, use, or sell any patented invention that may in any way be related thereto.

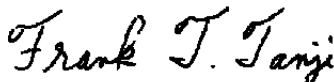
Qualified users may obtain copies of this report from the Defense Technical Information Center.

References to named commercial products in this report are not to be considered in any sense as an endorsement of the product by the United States Air Force or the Government.

This report has been reviewed by the Office of Public Affairs (PA) and is releasable to the National Technical Information Service (NTIS). At NTIS, it will be available to the general public, including foreign nations.

## APPROVAL STATEMENT

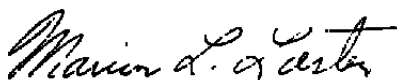
This report has been reviewed and approved.



FRANK T. TANJI, Captain, USAF  
Directorate of Technology  
Deputy for Operations

Approved for publication:

FOR THE COMMANDER



MARION L. LASTER  
Director of Technology  
Deputy for Operations

UNCLASSIFIED

SECURITY CLASSIFICATION OF THIS PAGE

## REPORT DOCUMENTATION PAGE

1a. REPORT SECURITY CLASSIFICATION <b>UNCLASSIFIED</b>			1b. RESTRICTIVE MARKINGS		
2a. SECURITY CLASSIFICATION AUTHORITY			3. DISTRIBUTION/AVAILABILITY OF REPORT Approved for public release; distribution unlimited.		
2b. DECLASSIFICATION/DOWNGRADING SCHEDULE			5. MONITORING ORGANIZATION REPORT NUMBER(S)		
4. PERFORMING ORGANIZATION REPORT NUMBER(S) AEDC-TR-85-16			7a. NAME OF MONITORING ORGANIZATION		
6a. NAME OF PERFORMING ORGANIZATION Arnold Engineering Development Center		6b. OFFICE SYMBOL (If applicable) DOT	7b. ADDRESS (City, State and ZIP Code)		
6c. ADDRESS (City, State and ZIP Code) Air Force Systems Command Arnold Air Force Station, TN 37389-5000			9. PROCUREMENT INSTRUMENT IDENTIFICATION NUMBER		
8a. NAME OF FUNDING/SPONSORING ORGANIZATION Arnold Engineering Development Center		8b. OFFICE SYMBOL (If applicable) DO	10. SOURCE OF FUNDING NOS		
8c. ADDRESS (City, State and ZIP Code) Air Force Systems Command Arnold Air Force Station, TN 37389-5000			PROGRAM ELEMENT NO 65807F	PROJECT NO	TASK NO
11. TITLE (Include Security Classification) Crushing Strength of Aluminum Oxide Agglom-			WORK UNIT NO		
12. PERSONAL AUTHOR(S) Gamble, R. A., Sverdrup Technology, Inc.					
13a. TYPE OF REPORT Final		13b. TIME COVERED FROM 4/83 TO 9/84		14. DATE OF REPORT (Yr., Mo., Day) July 1985	
15. PAGE COUNT 44					
16. SUPPLEMENTARY NOTATION Available in Defense Technical Information Center (DTIC).					
17. COSATI CODES			18. SUBJECT TERMS (Continue on reverse if necessary and identify by block number)		
FIELD	GROUP	SUB GR			
13	08		agglomerates aluminum oxide		
21	09	.2	solid propellants particle sampling		
			flow field bonding		
19. ABSTRACT (Continue on reverse if necessary and identify by block number)					
<p>Aluminum oxide, which is formed during combustion of aluminum-based solid propellants, condenses and solidifies in the exhaust flow to form sub-micron-size particles, which may then adhere together to form agglomerates. Particle sampling, which is required for motor performance or environmental impact investigations, is usually done using a probe placed in the supersonic exhaust flow field. The bow shock at the sample probe inlet will decelerate the gas flow which introduces a large velocity differential between the gas and particulate. This differential will result in a sudden increase in the aerodynamic drag on the agglomerates which may cause them to shear apart, thus altering the sample size distribution.</p> <p>In this effort, aluminum oxide agglomerates were formed and then crushed in order to estimate the magnitude of the interparticle forces binding the agglomerate together. The agglomerates were formed by tumbling commercially available aluminum oxide powder in a container, and strength was determined by measuring the load required to crush the agglomerate between two flat plates. Analysis indicated that rough, uniformly-shaped particles formed</p>					
20. DISTRIBUTION/AVAILABILITY OF ABSTRACT UNCLASSIFIED/UNLIMITED <input type="checkbox"/> SAME AS RPT <input checked="" type="checkbox"/> DTIC USERS <input type="checkbox"/>			21. ABSTRACT SECURITY CLASSIFICATION UNCLASSIFIED		
22a. NAME OF RESPONSIBLE INDIVIDUAL W. O. Cole			22b. TELEPHONE NUMBER (Include Area Code) (615) 454-7813	22c. OFFICE SYMBOL DOS	

DD FORM 1473, 83 APR

EDITION OF 1 JAN 73 IS OBSOLETE.

UNCLASSIFIED

SECURITY CLASSIFICATION OF THIS PAGE

UNCLASSIFIED

SECURITY CLASSIFICATION OF THIS PAGE

11. TITLE. Concluded.

erates (U)

20. ABSTRACT. Concluded.

the strongest agglomerates. The experimentally-derived particle bonding forces were in agreement with values predicted by the van der Waals force equation for closely-spaced spheres. Rocket exhaust particulates collected from a test facility exhaust processing system proved to be unusable because of impurities. Further studies are recommended with suitably collected and processed particulates.

UNCLASSIFIED

SECURITY CLASSIFICATION OF THIS PAGE

## **PREFACE**

The work reported herein was sponsored by Headquarters, Arnold Engineering Development Center (AEDC), Air Force Systems Command (AFSC). The results reported herein were obtained by Sverdrup Technology, Inc., a contract operator at AEDC, AFSC, Arnold Air Force Station, TN under AEDC Project No. D240. The work was conducted from April 1983 to September 1984, and the manuscript was submitted for publication on February 8, 1985.

The author wishes to thank Dr. Wheeler McGregor and Mr. Dave Van Dyke for their support and direction throughout this effort.

## CONTENTS

	<u>Page</u>
1.0 INTRODUCTION .....	5
2.0 THEORETICAL BACKGROUND .....	6
3.0 EXPERIMENTAL INVESTIGATION	
3.1 Agglomerate Generation .....	9
3.2 Crushing Strength Determination .....	10
4.0 RESULTS	
4.1 Agglomerate Analysis .....	12
4.2 Crushing Strength Analysis .....	13
5.0 CONCLUSIONS .....	15
REFERENCES .....	16

## ILLUSTRATIONS

<u>Figure</u>	<u>Page</u>
1. Schematic of Particle Probe in Supersonic Stream .....	19
2. Particle-Size and Agglomerate-Strength Regions in Which Various Binding Mechanisms Predominate (Ref. 11) .....	20
3. Crushing Strength of ZnO Agglomerates .....	21
4. Agglomerate Generation Apparatus .....	22
5. Agglomerate Crushing Apparatus .....	23
6. Scanning Electron Microscope Photographs of Unit Particle Shapes .....	25
7. Size Distribution of Agglomerates Tested .....	27
8. Solids Fraction Distribution of Agglomerates Tested .....	28
9. Interparticle Bonding Force Data .....	29
10. Unit Bonding Force versus Unit Crushing Force .....	30
11. Crushing Strength of Aluminum Oxide Agglomerates .....	31
12. Normalized Agglomerate Drag .....	32

## TABLES

1. Interparticle Bonding Forces .....	33
2. Powders Used In Agglomeration Experiments .....	34
3. Estimated Measurement Errors .....	35

**APPENDIX**

<b>A. Measurement Error Estimation Process .....</b>	<b>37</b>
<b>NOMENCLATURE .....</b>	<b>39</b>

## 1.0 INTRODUCTION

One of the exhaust products formed during combustion of aluminum-based solid propellants is aluminum oxide which ultimately takes the form of small solid particles. These unit particles may adhere or agglomerate together into larger particles as indicated by previous analysis of collected particulates (Ref. 1). The agglomerate formation location in the flow field, however, is not universally accepted to be in one specific region. Various authors have suggested the motor chamber (Ref. 2), the throat exit (Ref. 3), or farther into the exit cone (Ref. 4). The size of these particles is important because of their effects both on motor ballistic performance, and, in many cases, on the surrounding environment. Nonobtrusive sampling techniques are usually ineffective in measuring aluminum-oxide exhaust particulate because of the very high densities (Ref. 5). Sample extraction techniques are, therefore, required. The common method of injecting a sample probe in the exhaust flow, however, will disturb the flow field and introduce several potential errors in the ensuing data.

Girata (Ref. 1) identified several potential biases in his sampling work. Those associated with the sample probe are (1) material adhering to the probe inlet or sample lines, (2) agglomerates impacting the probe lip and breaking up, (3) the probe bow shock diverting the smallest particles away from the inlet, and (4) the agglomerates passing through the shock wave and shearing apart. The effects of the first item are easily determined by comparing the size distribution of material taken from the probe lip to that on the collection medium (e.g., witness stubs, filters, etc.). Agglomerate impaction on the probe should introduce a relatively small bias since the cross-sectional area of the probe lip is small compared to the inlet area. The remaining two items are caused by the sampling probe bow shock, which has an unknown and significant potential for altering the size distribution of the collected material. If the agglomerates do shear apart, then any material collected will falsely represent the actual free-stream conditions. In addition, information on the location of agglomerate formation in the nozzle cannot be obtained from collected particulate until the effects of the sample probe bow shock are fully known.

In previous work at AEDC, Forney et al. derived equations which provide insight on the effects of the bow shock on sampling probe collection efficiency and sampling biases. To further define the sampling phenomena, experimental data are needed on the strength of the aluminum-oxide agglomerate bonds and the effects of shock waves on agglomerate size.

This report is concerned with determining the strength of the interparticle agglomerate bonds, while subsequent work will be conducted on two-phase flow experimentation. The agglomerate generation and agglomerate crushing procedures are derived from previous work by Meissner et al. (Ref. 6) with zinc oxide. Data are presented and analyzed with applications to solid-propellant rocket motor plume sampling in mind.



## 2.0 THEORETICAL BACKGROUND

The exhaust products of an aluminum-based solid propellant include aluminum oxide ( $\text{Al}_2\text{O}_3$ ) which condenses and solidifies during discharge from the exhaust nozzle. Girata (Ref. 1) collected aluminum-oxide particulate using a probe mounted in the exhaust plume of a solid-propellant rocket motor. The experimental data indicate that this aluminum-oxide particulate consists of small ( $\sim 0.1 \mu\text{m}$ ) nearly spherical particles that combine to form agglomerates of various sizes (1 to  $5 \mu\text{m}$ ). If a sample extraction technique is used to collect these agglomerates for analysis, then the sampling technique may significantly bias the data. A schematic of a sampling probe in a supersonic flow is shown in Fig. 1. The nonuniform agglomerates in the two-phase flow field will respond to the sampling probe and bow shock based on their size, momentum, and strength. The small, lighter agglomerates will best follow the stream lines but may collide with and stick to the probe wall, decreasing the small particle concentration in the sample. The larger, heavier agglomerates outside of the entrained flow may have enough momentum to pass through the shock, cross the turning stream lines, and enter the probe, thus indicating a higher large-particle concentration that exists in the free stream. While these two possibilities have been previously addressed (Refs. 7, 8, and 9), the possible disintegration of agglomerates proposed by Girata has not been experimentally investigated.

A supersonic gas stream passing through a normal shock will decelerate to a subsonic velocity. Particulates in the gas stream will pass through the shock wave and experience a large velocity differential relative to the surrounding gas. The resulting drag on the particulate will be at a maximum immediately downstream of the shock wave and the particle drag will subside as the particle slows and the velocity differential vanishes. Forney calculated the free-stream Mach number which will impose the highest particle drag for a range of gas specific-heat ratios. For the specific-heat ratio range of 1.16 to 1.4, the maximum drag Mach number is between 2.3 and 2.4.

By definition, an agglomerate will break up if the external forces are greater than the combined interparticle forces binding the agglomerate together. This relationship is expressed as the ratio of the external force to the binding force and is known as the agglomerate Weber number,  $W_b$ . If the external forces are in the form of agglomerate drag,  $D$ , and the strength of the agglomerate is  $P$ , then we have

$$W_b = \frac{D}{P} \quad (1)$$

The criteria for breakup is when the Weber number exceeds unity.

Rumpf (Ref. 10), in his work on granulation of powders, defined the strength of an agglomerate composed of small uniform spheres as

$$\frac{P}{A_p} = \frac{\phi Z F}{\pi d_o^2}, \phi = \frac{Q_a}{Q_p} \quad (2)$$

where  $\phi$  is the agglomerate solid to total volume fraction,  $F$  is the particle bonding force function,  $P$  is the total force of adhesion,  $A_p$  is the cross-sectional area of the agglomerate,  $d_o$  is the unit sphere diameter, and  $Z$  is the coordination number. The derivation of this equation assumes that an agglomerate will fail when a cleavage plane is formed by a unit particle breaking one-half of its contacts with surrounding particles. The coordination number,  $Z$ , represents the number of points of contact that each unit particle has with surrounding particles. A coordination number of 2 would indicate a chain of particles while higher numbers represent more complex agglomerate structures. Rumpf demonstrates that for common coordination numbers (i.e., 2 through 12),  $Z(1 - \phi) \approx 3.1 \approx \pi$ . Equation (2) then simplifies to

$$\frac{P}{A_p} = \frac{\phi}{1 - \phi} \frac{F}{d_o^2} \quad (3)$$

Numerous particle bonding mechanisms have been discovered or invented. The strongest bonds are formed when the particles are heated and the particle surface is melted and fused with surrounding surfaces. Strong bonds are also formed when an adhesive binder is used. Other bonding mechanisms in order of decreasing strength include capillary forces, electrostatic forces, and van der Waals forces. Figure 2 (Ref. 11) shows the relative magnitudes of the bonding mechanisms with electrostatic forces included in the van der Waals force category. Figure 2 was generated from tensile strength test data for various materials. The test procedure consisted of firmly attaching agglomerates to a centrifuge rotor and collecting dislodged particles at various rotation rates. The centrifuge was enclosed and evacuated to eliminate aerodynamic drag with only centrifugal force causing tension on the agglomerates.

The compressive force required to shear an agglomerate will generally be higher than the tensile strength (Ref. 12). This results from the unit particles sliding past one another during compression, introducing a friction force. The standard test apparatus for compressive or crushing strength tests consists of a test specimen placed between parallel flat plates. This method will be used in the experiments reported herein, since compressive forces are present on an agglomerate in the decelerating flow field downstream of a normal shock.

Rumpf evaluated and summarized numerous equations pertaining to all types of particle bonding. The possible types of forces applicable to aluminum-oxide agglomeration are listed in Table 1, along with definitions, equations, constants, and typical values. Solid bridging of particles was not considered in this instance, since Girata's data indicated that this type of bonding was not present.

Van der Waals forces are attributable to the interaction of the surface atom electron orbits between adjacent surfaces or particles. As shown in Fig. 2, van der Waals forces are the weakest of the bonding mechanisms.

London and Heitler (Ref. 13) derived an expression applicable for small-sphere separation distances, while the equations are modified according to Lifshitz (Ref. 14) for larger distances. These forces are labeled  $F_{v1}$  and  $F_{v2}$ , respectively. An interparticle separation of 2,000 Å (0.2 μm) is the maximum distance for which the London-Heitler derivation applies.

Electrostatic bonding forces are possible when the particles are charged during formation or are exposed to an electron or ion charge after formation (i.e., a charged rocket motor exhaust). Experimental observations have shown that electrostatic forces can have a widely varied effect on the force of adhesion between particles. The magnitude of this effect is further enhanced by irregular particle surfaces and nonuniform charge distributions.

A surface film will develop on a particle when it is in contact with a condensable vapor. Rumpf found that agglomerates of particles can be bonded together through surface fluid bonding or negative capillary pressure in the fluid-filled space between particles. The first method, called the pendular state, assumes that fluid only exists at particle points of contact while the latter theory assumes that the entire inner agglomerate is fluid-filled. A combination of these two mechanisms, called the funicular state, has gas spaces present in the agglomerate void which are enclosed in a continuous network of liquid. Experimental work with iron ore agglomerates indicates that the funicular state provides the strongest form of liquid bonding.

The equations in Table 1 were derived for bonding forces between smooth, clean spheres. The constants, however, were evaluated from experimental data obtained from organic and inorganic particles that were moderately rough and spheroidal in shape. While the exact effects of surface roughness and particle shape are not known, the experimentally-derived constants are in acceptable agreement with theoretical values. Experimental measurements for specific applications are still necessary, however.

Meissner (Ref. 6), experimented with zinc-oxide powders. In his work, he painstakingly filtered the zinc-oxide powders to obtain unit particle sizes of 0.13 and 0.26 μm. These two

sizes of particles were tumbled separately for specified time periods to generate agglomerates with repeatable solids fractions. These spherical agglomerates were then crushed using the accepted method of placing the agglomerate between two flat plates. The resulting data are shown in Fig. 3 and are presented using an exponential function of the solids fraction. Meissner's conclusion, which is also imbedded in Rumpf's work, is that the agglomerate strength is a unique function of the unit particle diameter,  $d_p$ , the agglomerate diameter,  $d$ , and the volume fraction of solids,  $\phi$ .

Aluminum-oxide powder should have a similar function relating  $d_p$ ,  $d$ , and  $\phi$ . Agglomeration experiments were conducted to determine this relationship and to attempt to identify the interparticle forces present in the agglomerates.

### 3.0 EXPERIMENTAL INVESTIGATION

#### 3.1 AGGLOMERATE GENERATION

The apparatus used to generate the agglomerates is shown in Fig. 4. This apparatus consisted of a 2-l glass bottle and stopper, a four-padded-roller support stand, a small drive motor, and a variac for setting the tumbling rates. The drive motor was connected in parallel with the tumbling bottle with an oversize rubber O-ring placed over the mid-section of the bottle. A small teflon support pad was positioned over the bottle stopper to prevent the bottle from moving axially. Bottle rotation speeds were calculated by measuring elapsed time for an arbitrary number of bottle revolutions.

Powder was obtained from several sources. Table 2 identifies the chemical analysis and size range of each of the powders used as advertised by the manufacturer. The RE sample was taken from a collection pit at an AEDC test cell. The material collected was a sample of the particulate which had passed through an iron and cement exhaust diffuser system during previous tests of solid-propellant rocket motors. The collected sludge was dried, processed, and analyzed at the AEDC Chemical Laboratory. Calcium carbonate powder was also included because it was readily available, appeared similar to the finer-sized aluminum-oxide powders, and would provide an agglomerate strength comparison. Acquisition of a similar-size zinc-oxide powder was not possible; current manufacturers could supply nothing in a comparable size range.

Samples of each powder were atomized, placed on a witness stub, and examined and photographed with a Scanning Electron Microscope (SEM). A chemical analysis of each powder was performed by using an energy dispersive spectrometer connected to the SEM.

Agglomerate generation was attempted for each of the powders listed in Table 2. Tumbling rates and duration were varied from 40 to 250 rpm and from 20 min to 26 hr,

respectively. Best results were obtained by setting jar rotation at 80 to 90 rpm. All powders were tumbled before and after open-air drying on a hot plate in order to determine any noticeable effects of moisture content on agglomerate formation.

Most of the powders tested would not agglomerate. These powders tended to slide on the tumbling jar wall until a *critical* jar rotation speed was reached. At this point, the powder would start to tumble in the jar. One of two events would then occur. Either the powder mass would return simply to sliding on the wall, or the powder would start adhering to the jar wall in increasing amounts until all powder was caked-on in a continuous cylinder. This latter event would begin at times varying from a few seconds to over 30 min after tumbling began. The reason for this event is unknown. The caking was not noticeably affected by the pretest drying process. A tesla generator was used on both the interior and exterior surfaces to neutralize any static charge buildup between the jar and powder, but with no apparent effect.

Agglomeration of three of the powder samples was accomplished. These were the Micro-Abrasives samples and the RE material. Of these three, the rocket exhaust residue was the least pure and tended to form the largest, most fragile agglomerates (~ 6 mm). The agglomerate surface was noticeably rough. The less pure Micro-Abrasives materials (M-1-97) contained approximately 3-percent impurities and also formed fragile agglomerates. Attempts to remove many of these two types of agglomerates from the tumbling apparatus ended in their destruction.

The most success was obtained with the M-1-99 Micro-Abrasives sample. At any one time, the number of agglomerates in the previous two materials stayed relatively constant, whereas in the M-1-99 material, the number of agglomerates kept increasing. This held true until all powder had agglomerated, and further tumbling tended to narrow the size distribution. These agglomerates were smooth spheres or spheroids and dissection indicated a concentric sphere structure with the inner sphere also having a smooth surface.

### **3.2 CRUSHING STRENGTH DETERMINATION**

The M-1-99 agglomerates were chosen for crushing strength experiments because they were from the purest powder and had a measurable crushing strength with the apparatus used. It was decided that the RE sample agglomerates were too contaminated to give meaningful results and the M-1-97 agglomerates were too fragile to handle.

The M-1-99 agglomerates were arbitrarily categorized by size, and several from each category were removed for experimentation. The agglomerates were weighed to the nearest

0.01 mg using a microscale and measured to the nearest 5  $\mu\text{m}$  using a microscope. From this data, the solids fraction,  $\phi$ , of each agglomerate was determined.

A crushing apparatus (Fig. 5) was assembled to load the agglomerates. This apparatus consisted of a thick circular piece of polished glass used as a base plate, 2 hinged microscope slides, a 10-cm tall plastic cylinder epoxied to one end of one slide, and a vertically-supported graduated buret. Individual agglomerates were placed on the base plate and centered under the slide and cylinder.

The buret stopcock was adjusted so that water would slowly drip from the buret into the open cylinder until the agglomerate failed. Pre- and posttest water levels in the buret provided a measure of the mass of water required to crush the agglomerate. In most cases, preweighed pieces of electrical wire were placed in the cylinder prior to testing in order to avoid filling the cylinder prior to agglomerate failure. In every instance, agglomerate failure occurred suddenly without any premature flattening of the agglomerate. Any prior deformation of the agglomerate would be easily noted in the movement of the relatively long cylinder.

Occasionally, a static charge would build up on the glass base plate and make positioning of the agglomerates difficult. Spray static remover was applied to the glass and slides to alleviate the problem.

A list of the measured parameters of this experiment is shown in Table 3. Also shown in Table 3 are possible factors affecting the accuracy of the measurements along with the maximum estimated error for each factor. Appendix A is a brief description of the error estimation process.

Thirty-eight agglomerates were successfully measured and crushed in this experiment. A larger data base was planned for statistical purposes; however, agglomerate handling during the various processes destroyed many of the agglomerates.

The crushing strength apparatus used here does not duplicate the distributed pressure loading that an agglomerate would actually experience after passing through a normal shock wave. Some previous experiments have used compressive mats to provide a more uniform loading (Ref. 11). In either case, failure will occur when a unit particle forms a cleavage plane with surrounding particles, as previously assumed. Evidence for this assumption is provided in the abrupt manner in which the agglomerates fail. The point-loading apparatus will, therefore, still permit measurement of the interparticle bonding force.

## 4.0 RESULTS

### 4.1 AGGLOMERATE ANALYSIS

The chemical analysis of the powders used in these experiments is included in Table 2, and a photograph of the typical unit particle shapes for each powder is shown in Fig. 6. Examination of each photograph shows that the particle shapes vary from long spikes to jagged cubes to smooth spheroids. Figures 6a through c are of the three Buehler powders that would not agglomerate. These unit particles tended to be relatively smoother and more uniform compared to the other powders. The calcium carbonate (Fig. 6d) also would not agglomerate even though a wide distribution of particle sizes is evident. The abundance of the extremely large particles (3 to 4  $\mu\text{m}$ ) may interfere with the agglomeration process in this powder.

The particles shown in Figs. 6e through g are from powders that did agglomerate. Figure 6e shows the unit particles that formed the strongest agglomerates. These particles appeared to be uniformly sized, similar to the Buehler powders, but more varied in shape. It is this variety in shape that may give these agglomerates their strength. The other two agglomerating powders (Figs. 6f and g) also have nonuniform shapes, but their size distribution is wider. The chemical analysis of the various powders verified the manufacturer's stated purities. The chemical purity did not appear to affect the agglomeration characteristics of these powders. An exception to this is possible in the RE sample if the interparticle bonding forces were affected by the varied elemental composition.

The size distribution of the agglomerates measured with a microscope and used in the crushing experiment is shown in Fig. 7. There is an unexpected gap in the measured size distribution of these agglomerates. As Fig. 7 shows, most of the agglomerates were fairly evenly distributed in size between 0.8 and 1.4 mm, except for the single agglomerate measuring 1.05 mm. At the beginning of the sample selection process, the agglomerates were crudely sized by sifting through different makeshift sieves, and then equal numbers of agglomerates were chosen from each of the four size categories. One of the sieve sizes was slightly over 1 mm. A bias in the size distribution could have been created by separating the 1 to 1.1-mm-size agglomerates into two size categories, thereby reducing the probability of that size being chosen.

The solids fraction distribution of the sampled agglomerates is shown in Fig. 8. As in the size distribution, there is a depressed region in the middle of the distribution. The solids fraction data were plotted against the agglomerate diameter values, but no significant trend or correlation was found.

## 4.2 CRUSHING STRENGTH ANALYSIS

The interparticle bonding force function,  $F$ , was calculated for each agglomerate using Eq. (3) and measurement data. A unit particle diameter of  $0.8 \mu\text{m}$  was used for all calculations and was based on average particle measurements on the SEM. Figure 9 shows the resulting bonding force function as a function of the agglomerate solids fraction. A least-squares linear fit of the data indicates the trend of decreasing bonding force with increasing solids fraction and constant crushing force. This is expected, since a denser agglomerate will have a higher coordination number and each particle bond will be weaker.

The unit bonding force function,  $F/d_o$ , is plotted for values of the unit crushing force,  $P/A_c$ , in Fig. 10. The least-squares linear fit and  $2\sigma$  confidence bands shown in Fig. 10 indicate that the crushing force and solids fraction data used in Eq. (3) to generate the bonding force function provide a good correlation.

The average value of the bonding force function shown in Fig. 9 is  $1.2 \times 10^{-2}$  dyne. Comparison of this value with the order-of-magnitude predictions by Forney shown in Table 1 indicates that any of the types of bonding mechanisms listed could possibly be responsible for the agglomerates' strength. The average value of the unit crushing force data shown in Fig. 10 is  $1.4 \times 10^6$  dyne/cm<sup>2</sup>. For an agglomerate in tension with  $0.8\text{-}\mu\text{m}$  unit particles, Fig. 2 incorrectly indicates that the bonding mechanism is attributable to capillary or surface-film forces. Two reasons are given to support this statement. For these two reasons, the conclusion reached is that capillary forces are not the bonding mechanism in these aluminum-oxide agglomerates.

The first reason deals with the manner in which the agglomerates were formed. The literature addressing the formation of various liquid bonds routinely discusses the addition or removal of liquid during the agglomeration process as the basic factor in agglomerate strength. These aluminum-oxide agglomerates were formed by only tumbling powder in a sealed jar.

The second reason is in the quantity being measured. As previously stated, the compressive strength of an agglomerate is expected to be greater than the tensile strength because of the friction forces between the unit particles. As stated by Rumpf (Ref. 12), however, this is an unknown nonlinear relationship dependent upon particle size, particle shape, and overall agglomerate strength. The van der Waals capillary forces boundary line in Fig. 2 should, therefore, be adjusted upward by an undetermined amount.

Electrostatic forces may be the bonding mechanism. A tesla generator was used to discharge a strong electron spark to an agglomerate with no apparent effect. If electrostatic



forces were the bonding mechanism, then a strong unipolar charge might have weakened or destroyed the particle bonds. This test is inconclusive, however, since the tesla generator may only affect the surface charge of the agglomerate and not the internal bonding structure.

A direct test for van der Waals forces was not devised, so it is uncertain as to which type of bonding mechanism is responsible for the strength of the agglomerates. However, the electrostatic force value shown in Table 1 is for smooth spheres and, as stated previously, may be greatly increased because of particle surface irregularities. Since these particles have irregular surfaces, electrostatic bonding would produce higher values of bonding force than were determined experimentally. Therefore, by the process of elimination, the London-Heitler-type van der Waals forces ( $a < 2,000 \text{ \AA}$ ) is the primary bonding mechanism.

The experimental data are also presented in the format of Meissner in Fig. 11. The use of an exponential function of the solids fraction is plausible since manipulation of Eq. (3) yields

$$\frac{P/A_p}{F/d_0^2} = \frac{\phi}{1 - \phi} \quad (4)$$

which is an approximation of an exponential term. Various values of the constant in the exponential term were evaluated in an attempt to improve the least-squares fit of the data. The  $2-\sigma$  confidence bands shown in Fig. 11 indicate the ability of the exponential function to fit the data; however, there is a large variance in the slope because of the nature of the data. The scatter in the aluminum-oxide data in Fig. 11, in comparison to the zinc-oxide data in Fig. 2, is probably attributable to the differences in the unit particle size distribution and the averaged data points of Meissner compared to the unaveraged data of this report.

The free-stream Mach number which will result in a normal shock strong enough to break these agglomerates is now considered. Forney developed equations for predicting agglomerate breakup in terms of the free-stream Mach number and other gas parameters. Modifying Eq. (1) to account for aerodynamic drag and crushing strength data results in

$$W_b = \frac{D}{P} = \frac{D/A_p}{P/A_p} = \frac{P_0 C_D g(M_1, \gamma)}{P/A_p} \quad (5)$$

where  $P_0$  is the free-stream pressure,  $C_D$  is the agglomerate drag coefficient, and  $g(M_1, \gamma)$  is a nondimensional function of free-stream Mach number and specific-heat ratio relating gas properties across a normal shock wave.

Forney plotted the normalized agglomerate drag,  $D/P_0 A_p [= C_D g(M_1, \gamma)]$ , for various values of free-stream Mach number and agglomerate Knudsen number function. The

agglomerate Knudsen number is defined as the ratio of the mean free path of the gas to the agglomerate diameter. A complete derivation and description are given by Forney which result in a lumped parameter,  $d\rho_0/k$ , where  $\rho_0$  is the gas density and  $k$  is a constant ( $8.46 \times 10^{-9}$  gm/cm<sup>2</sup>) calculated from the gas constant,  $R$ , and Sutherland's constant,  $T_0$ . This parameter is proportional to the inverse of the agglomerate Knudsen number and is used by Forney as an indicator of normalized agglomerate drag. A set of curves similar to those of Forney is shown in Fig. 12. Curves for higher values of constant  $d\rho_0/k$  were added because of the larger agglomerate diameters for this study. By assuming the gas parameter values shown in Fig. 12 and further assuming a free-stream total pressure of  $5.5 \times 10^7$  dyne/cm<sup>2</sup> (800 psia), and a Weber number of 1, one can determine a Mach number range which should cause the agglomerate to fail. For the assumed conditions, the drag function  $D/P_0A_p$  is  $2.5 \times 10^{-2}$ , and the value of the lumped parameter  $d\rho_0/k$  is  $7 \times 10^4$ . From Fig. 12, the corresponding Mach number range for probable agglomerate breakup is approximately 1.4 to 3.4. An experiment to verify this calculation was not performed. The acceleration forces required to establish a supersonic agglomerate velocity would be greater than the agglomerate crushing strength and would cause agglomerate failure.

## 5.0 CONCLUSIONS

This investigation was conducted to provide experimental data on the strength of aluminum-oxide agglomerates. While the agglomerates studied were not generated by an environment similar to a solid-propellant rocket motor firing, the data obtained are unique and provide a basis for further studies. The conclusions are as follows:

1. Based upon SEM photographs and experience, it appears that uniformly-sized, rough-edged, unsymmetrical particles form the strongest, most spherical agglomerates. The uniform spherical particles used in this effort would not agglomerate. Agglomerates were randomly selected for crushing strength experiments; however, a preliminary sizing process may have slightly biased the size distribution of the agglomerates used.
2. The interparticle bonding force values were calculated from crushing force, size, and solids fraction data. These force values were in agreement with the predicted estimates by Forney for each of the bonding mechanisms considered; however, van der Waals forces are considered the most probable force of adhesion. This is encouraging, since the equations and experimental constants were derived for spherical, or nearly spherical, unit particles and the aluminum-oxide particles used here were randomly shaped.
3. A comparison of the crushing strength of these agglomerates with generalized experimental values of tensile strength proved invalid. An experimental program

to obtain compressive strength data for direct comparison to Rumpf's tensile strength tests is required.

4. The calculated unit bonding force ( $F/d_o$ ) was favorably correlated with the unit crushing force data ( $P/A_p$ ). A plot relating the unit crushing force to a function of the solids fraction was generated in an attempt to relate the aluminum-oxide data to previous work with zinc oxide. While similar trends were apparent, the differences in powder preparation and amount of data obtained preclude further comparisons.
5. Further studies are required with characterized agglomerates in a supersonic two-phase flow field to determine experimentally the onset of agglomerate breakup. In addition, studies with actual rocket-exhaust particulate are required. The RE sample material used in these experiments was collected after passing through an iron and cement exhaust diffuser system, and the impurities from these materials substantially weakened the agglomerate bonds. Now that a proven procedure for determining particle bonding forces of aluminum-oxide agglomerates is available, a more direct collection of exhaust particulate in the nozzle flow field is warranted in order to duplicate and verify these results. Data from further tests will then provide a basis for determining the sample distribution bias caused by a sample probe bow shock.
6. A calculation was performed using Forney's equations which compared agglomerate strength to the drag forces present in a decelerating flow field. The calculations indicate that an average agglomerate generated in this study would survive passage through a normal shock, if the free-stream Mach number is less than 1.4 or greater than 3.4, and assuming the agglomerate was initially traveling at the gas stream velocity. The forces required to accelerate such large agglomerates realistically to supersonic velocity, however, would probably cause their destruction.

## REFERENCES

1. Girata, Jr., P. T. and McGregor, W. K. "Particle Sampling of Solid-Propellant Rocket Motor (SRM) Exhausts in High-Altitude Test Cells." AIAA Paper No. 83-0245, January 1983.
2. Cheung, Henry and Cohen, N. S. "Performance of Solid Propellants Containing Metal Additives." *AIAA Journal*, 3, 1965, pp. 250-257.

3. Marble, F. E. "Droplet Agglomeration in Rocket Nozzles Caused by Particle Slip and Collision." *Astronautica Acta*, 13, 1967, pp. 159 - 166.
4. Crowe, C. T. and Willoughby, P. G., "A Study of Particle Growth in a Rocket Nozzle." *AIAA Journal*, 5, 1967, pp. 1300 - 1304.
5. McGregor, W. K. "Assessment of In-Situ Diagnostics for Application to Rocket Propulsion Problems," AFRPL-TR-78-62, June 1979.
6. Meissner, H. P., Michaels, A. S., and Kaiser, R. "Crushing Strength of Zinc-Oxide Agglomerates." *I&EC Process Design and Development*, 3, 1964, pp. 202 - 205.
7. Forney, L. T. "Aerosol Impactor for Large Sample Volumes." *Rev. Sci. Instrum.*, 10, 1976, pp. 1264 - 1269.
8. McFarland, A. R., Ortiz, C. A., and Bertch, Jr., R. W. "Particle Collection Characteristics of a Single-Stage Dichotomous Sampler." *Environ. Sci. Technol.*, 12, 1978, pp. 679 - 682.
9. Friedlander, S. K. *Smoke Dust and Haze: Fundamentals of Aerosol Behavior*. John Wiley Press, N. Y., 1976.
10. Rumpf, H. "Fundamentals and Methods of Granulation." *Chem. Ign. Tech.*, 30, 1958, pp. 144-158.
11. Rumpf, H. "The Strength of Granules and Agglomerates." *Agglomeration*, W. A. Knepper, ed., New York: John Wiley Press, 1962, pp. 382 - 403.
12. Orr, Jr., C. *Particulate Technology*. New York: Macmillan Company, 1964.
13. London, F. "The General Theory of Molecular Forces." *Transactions of the Faraday Society*, 33:8 - 26, 1937.
14. Lifshitz, E. M. "The Theory of Molecular Attractive Forces Between Solids." *Soviet Physics - Journal of Experimental Theoretical Physics*, 2:73 - 83, January, 1956. Translation from the Russian published by American Institute of Physics, R. T. Beyer, ed.

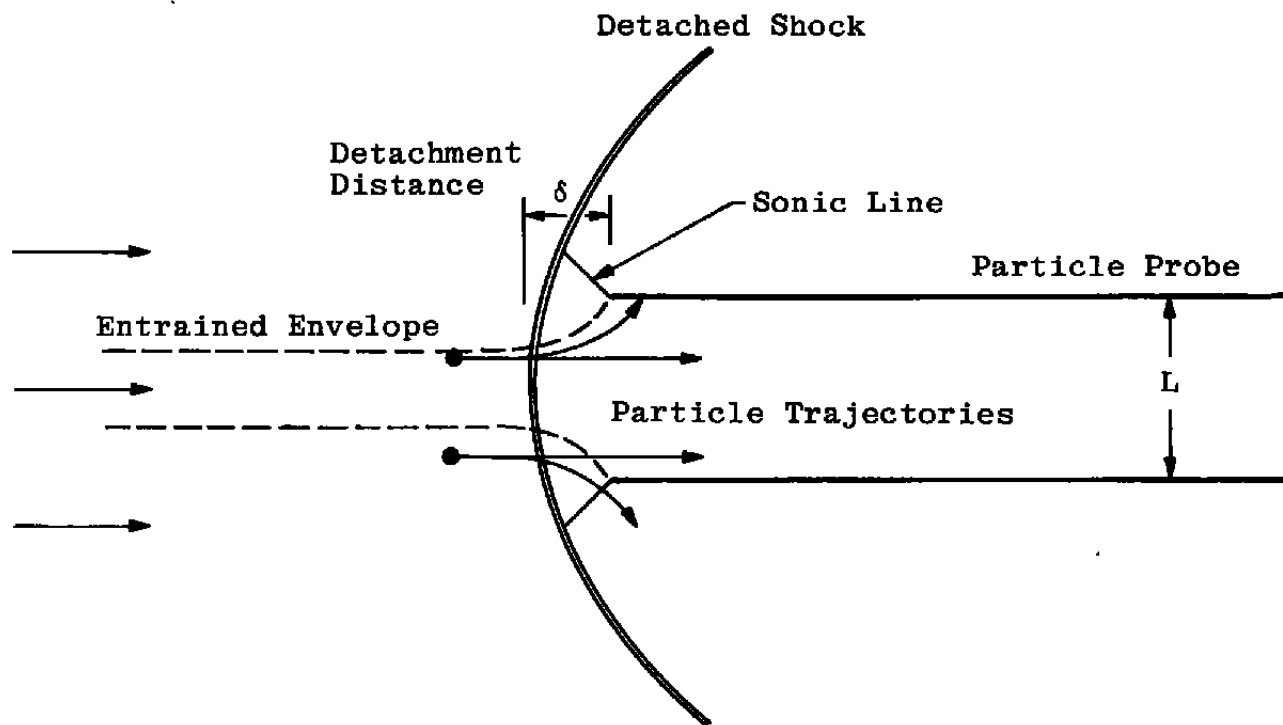
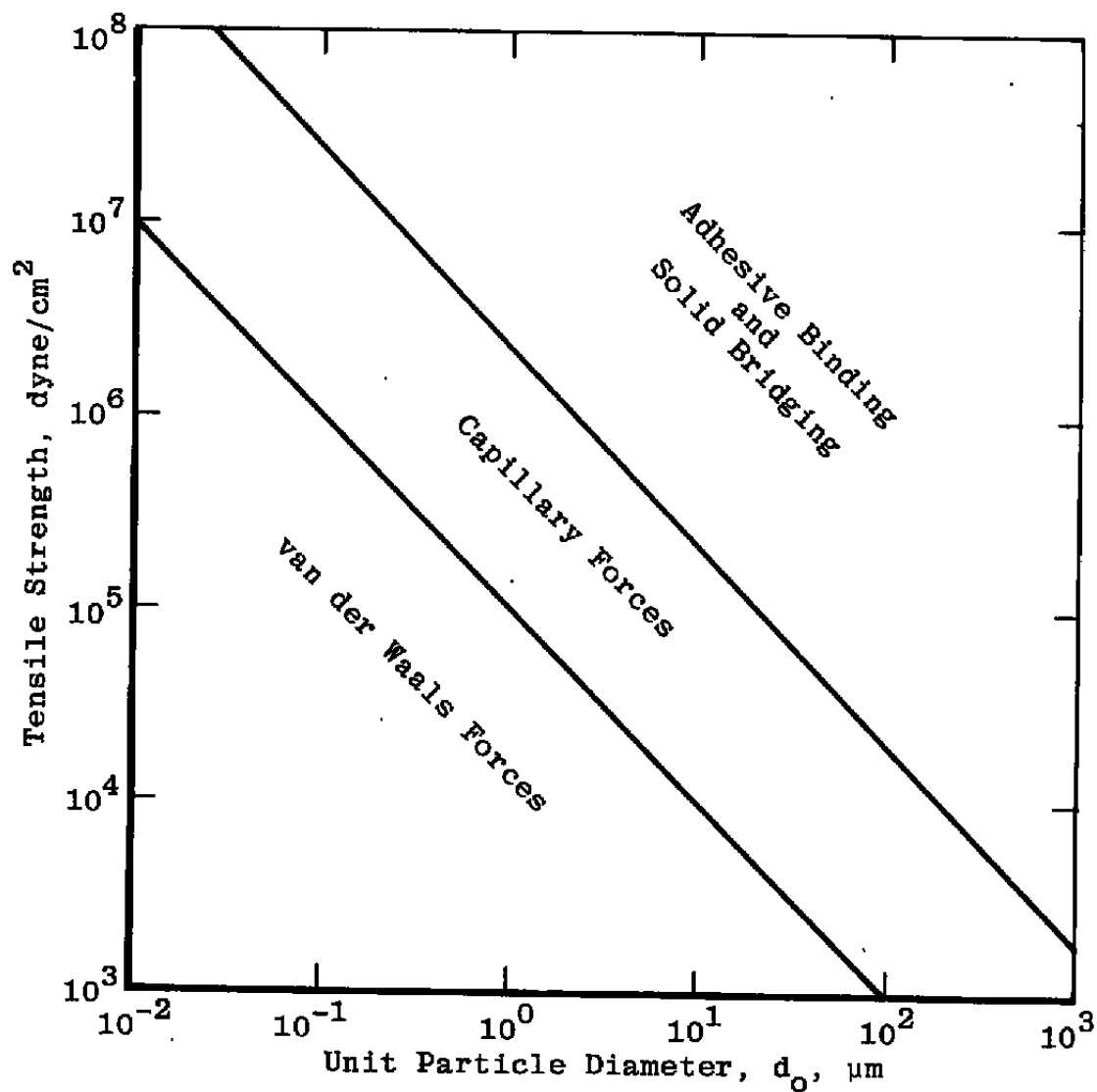


Figure 1. Schematic of particle probe in supersonic stream.



**Figure 2. Particle-size and agglomerate-strength regions in which various binding mechanisms predominate (Ref. 11).**

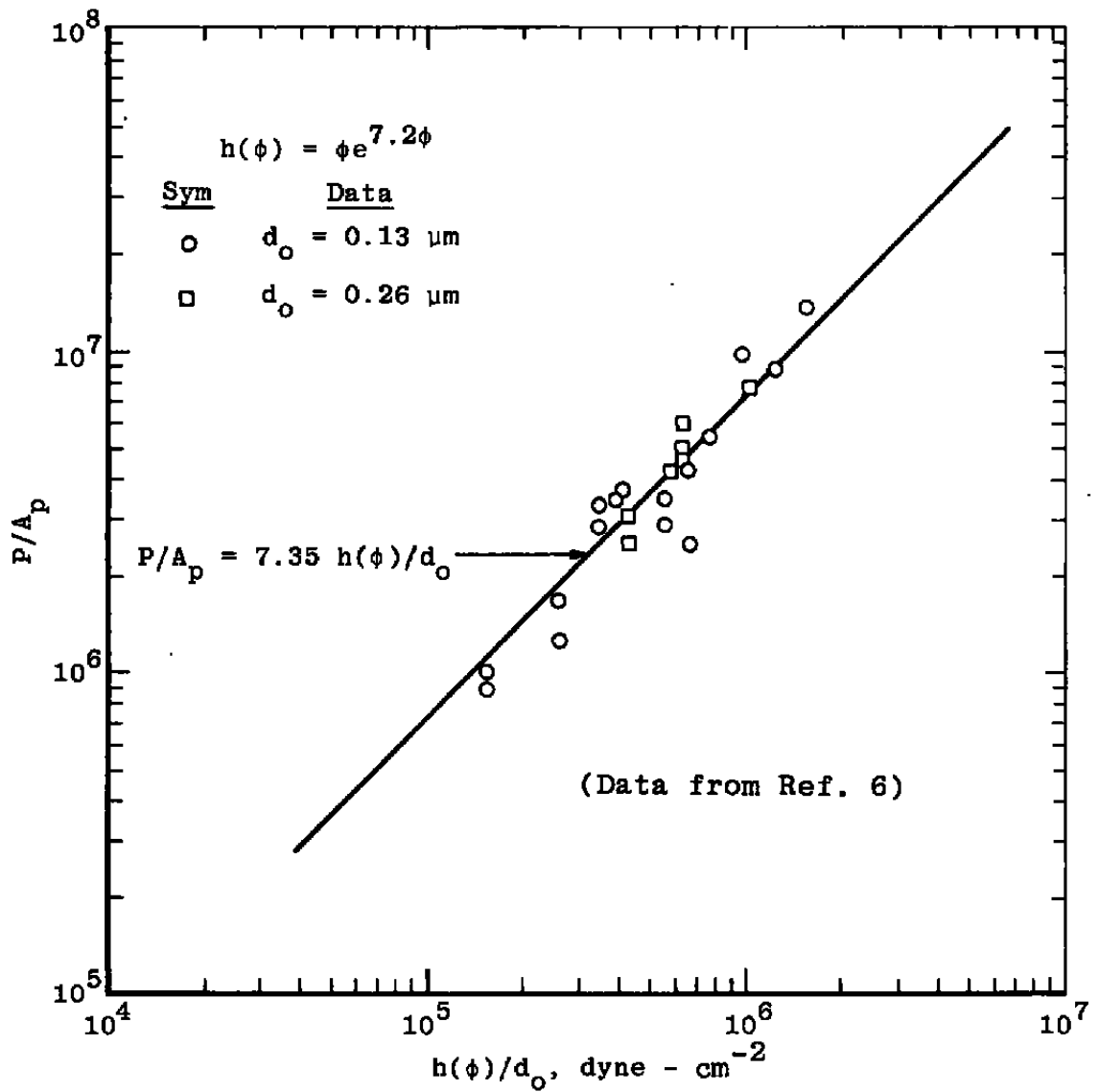
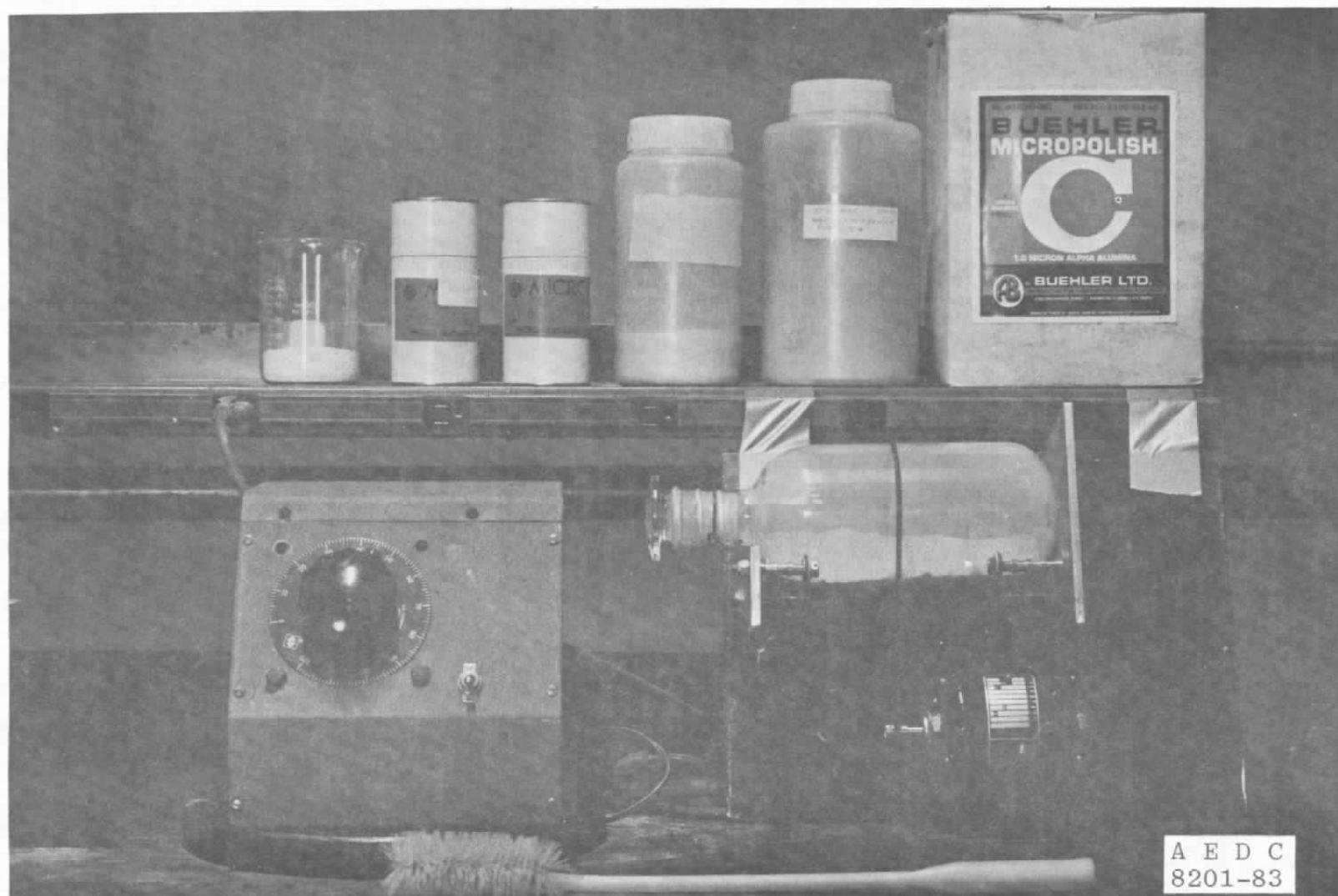
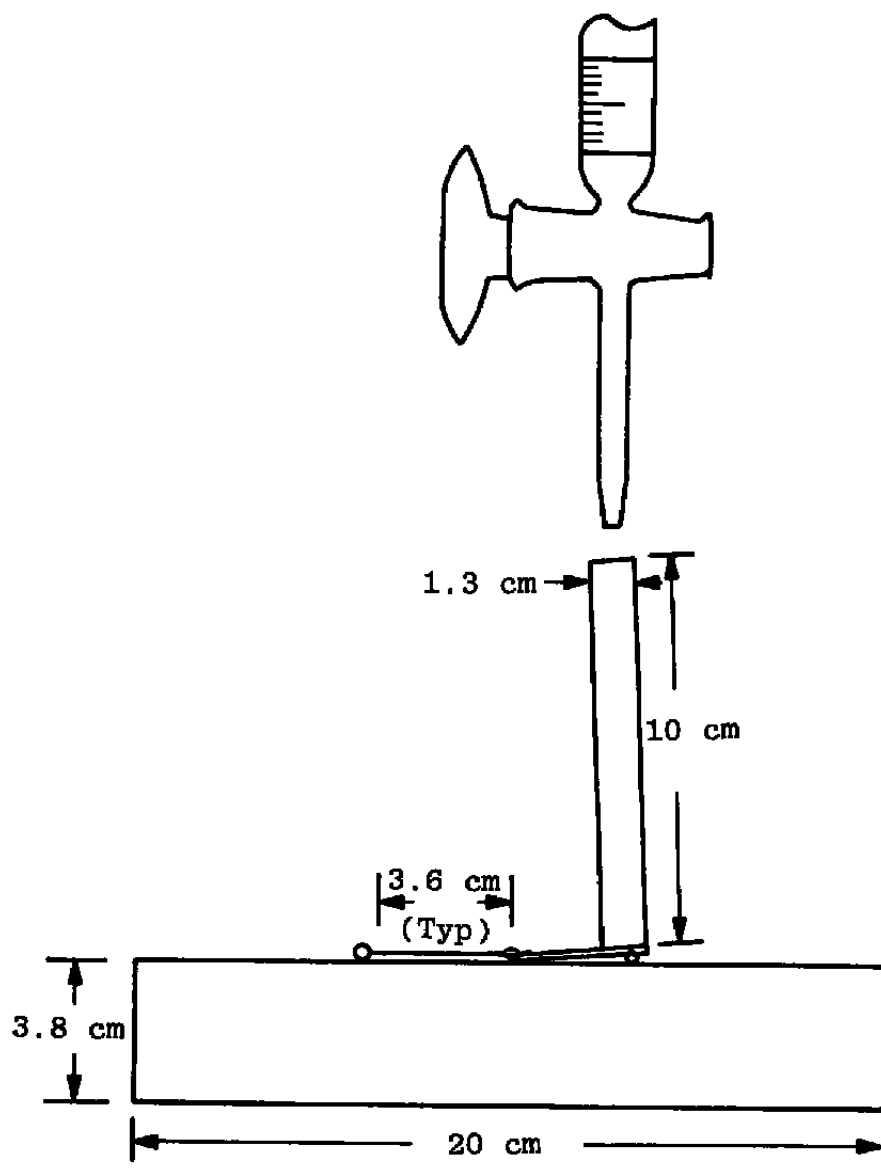


Figure 3. Crushing strength of ZnO agglomerates.



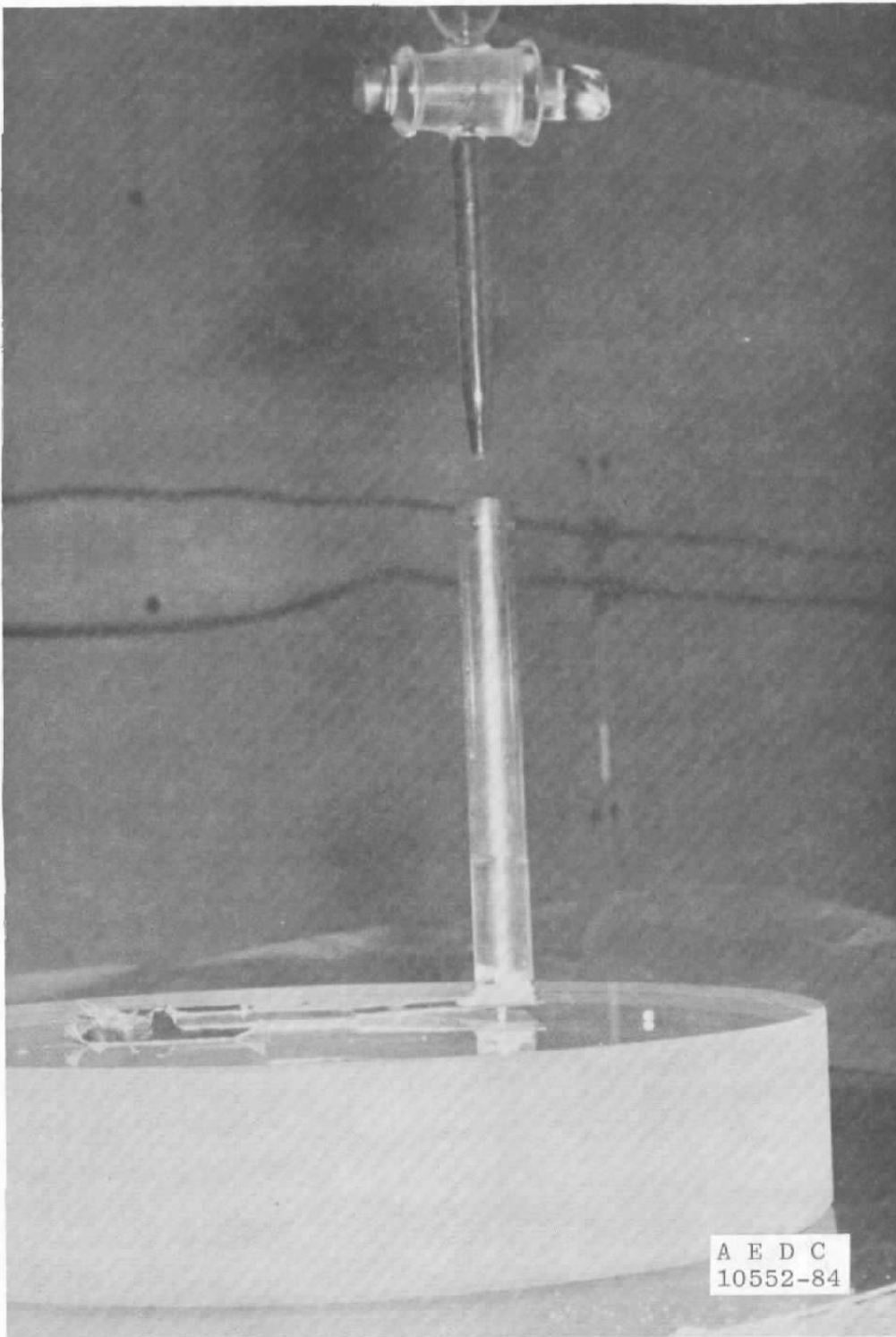
**Figure 4. Agglomerate generation apparatus.**



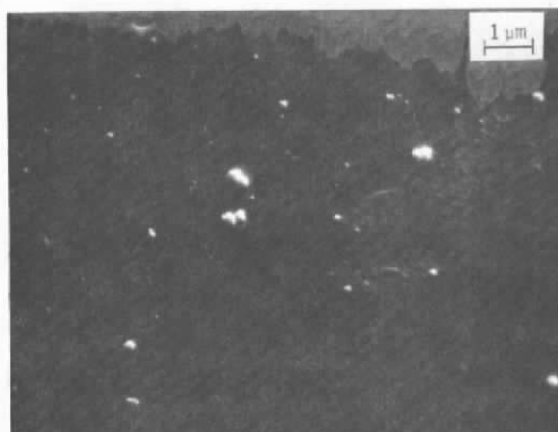


a. Schematic

Figure 5. Agglomerate crushing apparatus.



**b. Photograph  
Figure 5. Concluded.**



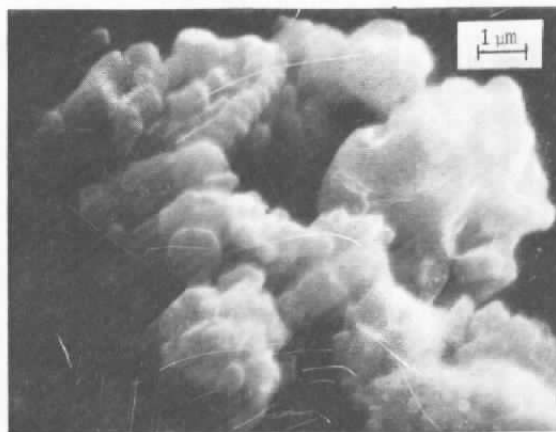
**a. 0.005- $\mu$ m aluminum oxide powder (B-0.05)**



**b. 0.03- $\mu$ m aluminum oxide powder (B-0.3)**



**c. 1.0- $\mu$ m aluminum oxide powder (B-1.0)**



**d. 1.0- $\mu$ m calcium-carbonate powder (C)**

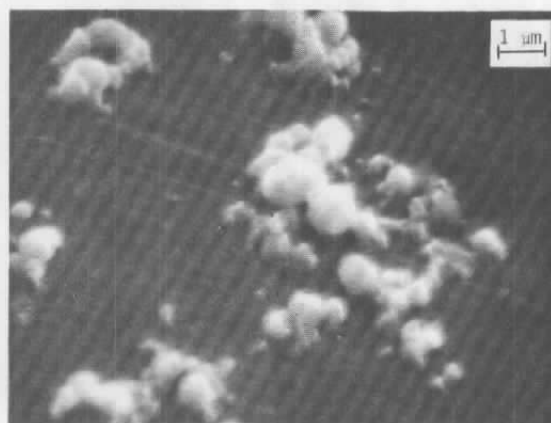
**Figure 6. Scanning electron microscope photographs of unit particle shapes.**



**e. 1.0-μm aluminum oxide powder (M-1.0-99)**



**f. 1.0-μm aluminum oxide powder (M-1.0-97)**



**g. Processed material from rocket motor firing (RE)**

**Figure 6. Concluded.**

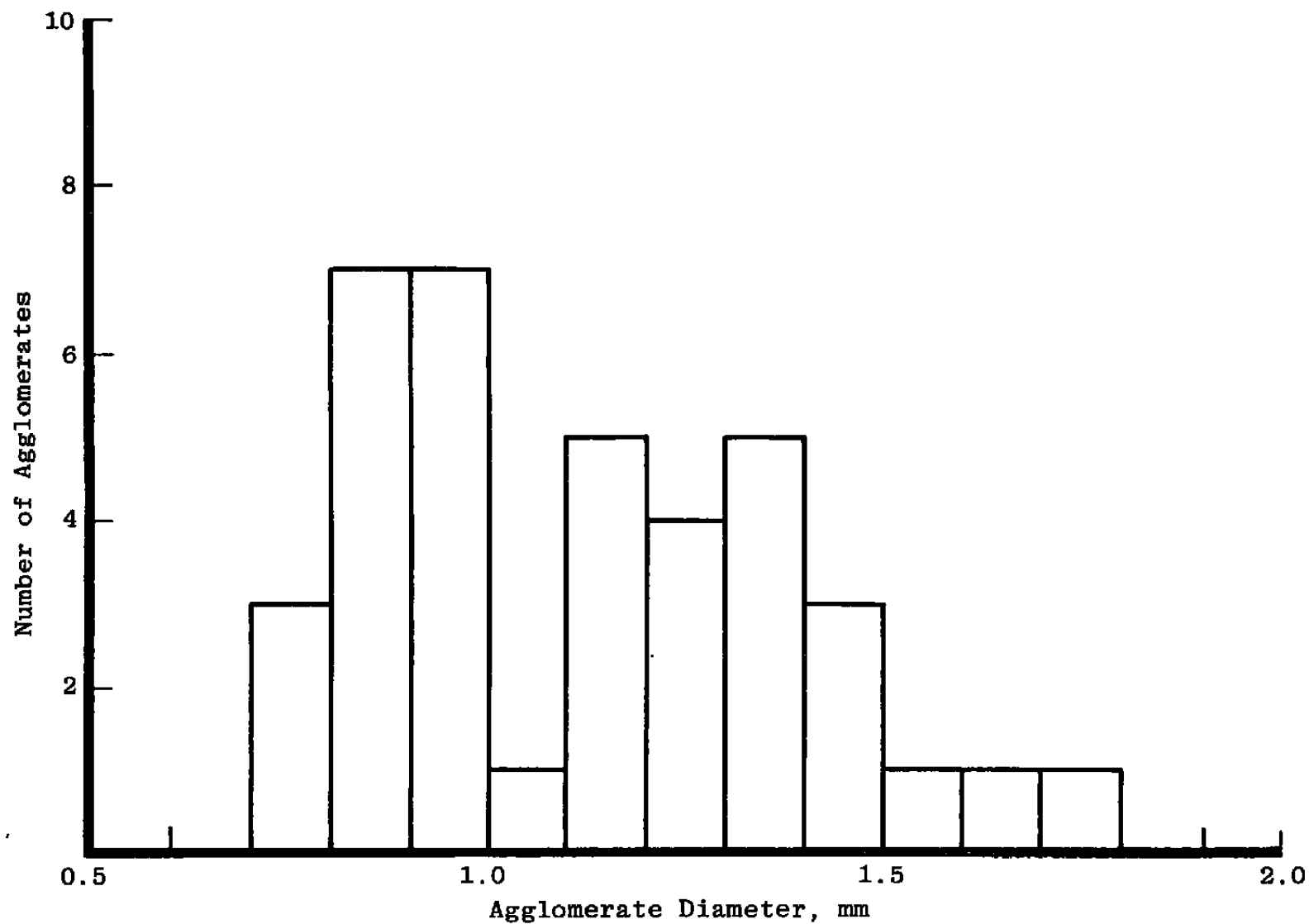


Figure 7. Size distribution of agglomerates tested.

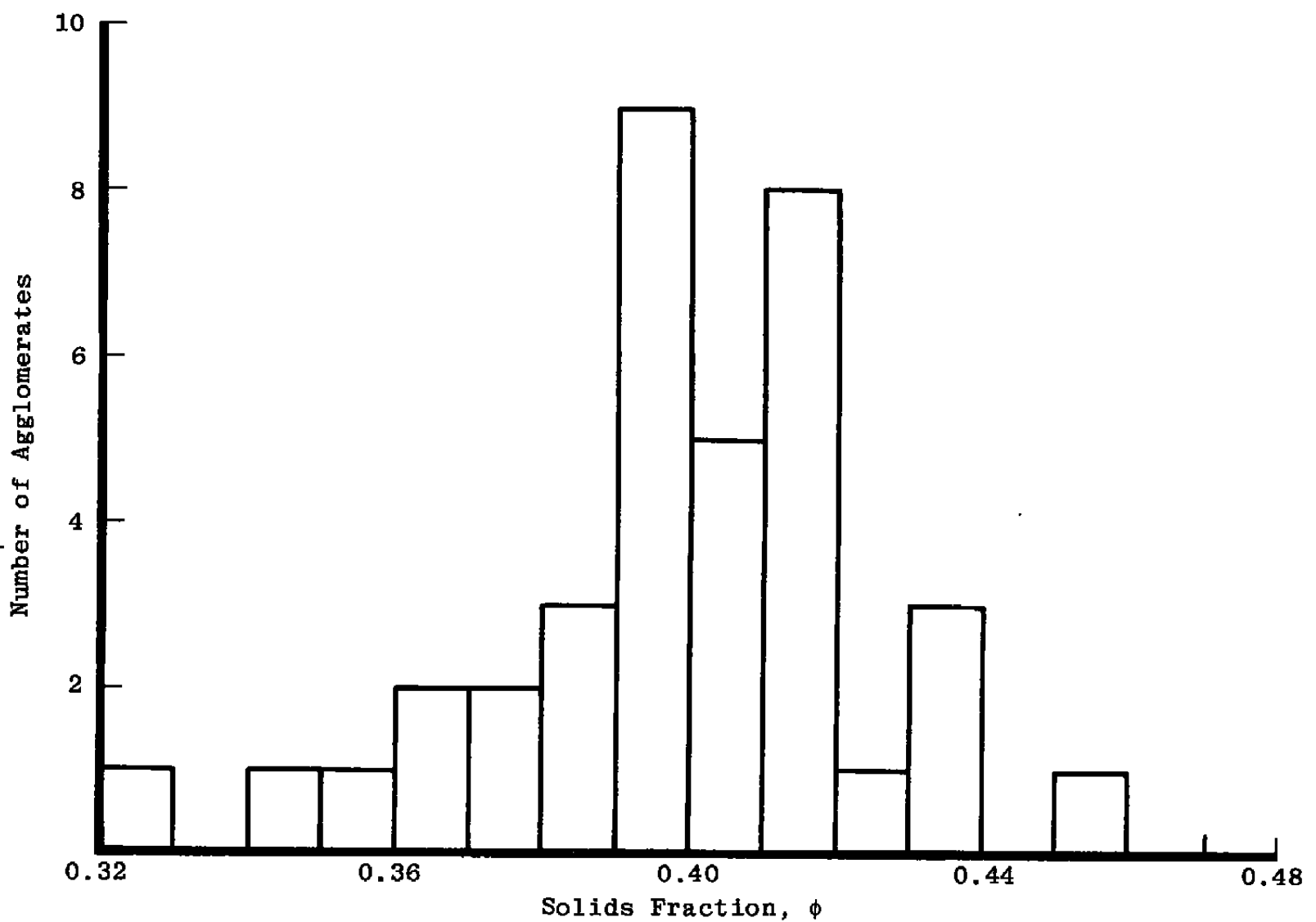


Figure 8. Solids fraction distribution of agglomerates tested.

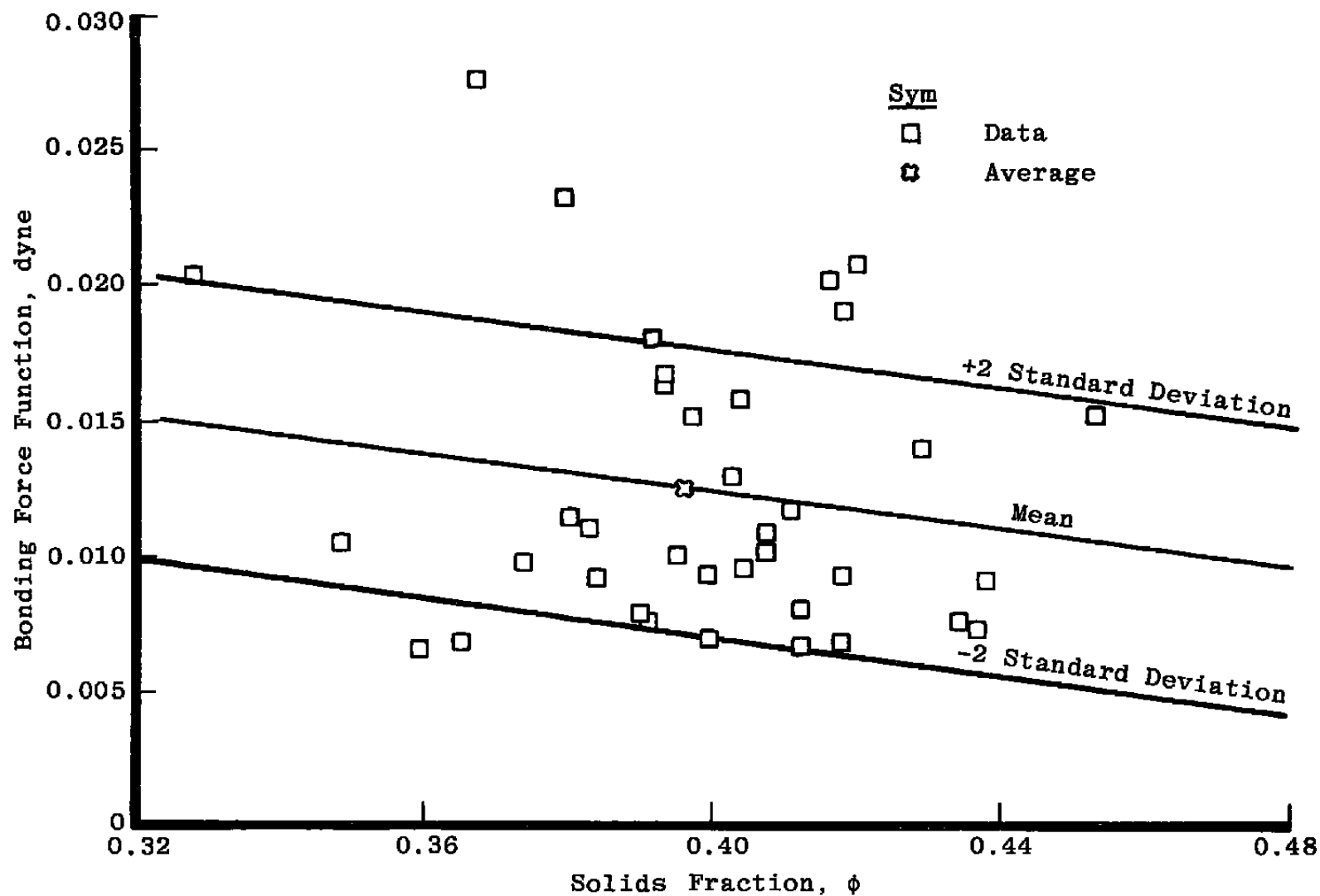


Figure 9. Interparticle bonding force data.

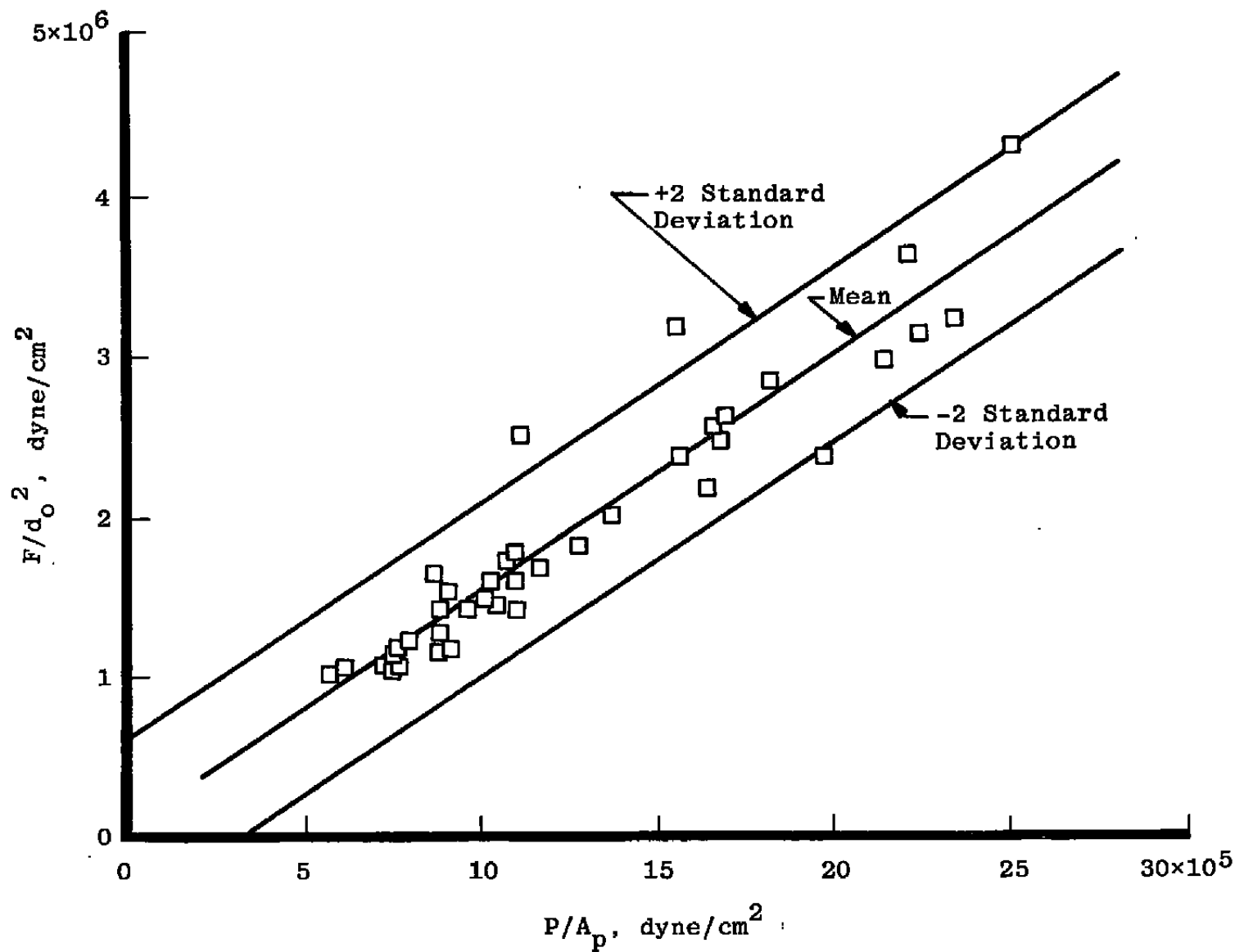


Figure 10. Unit bonding force versus unit crushing force.



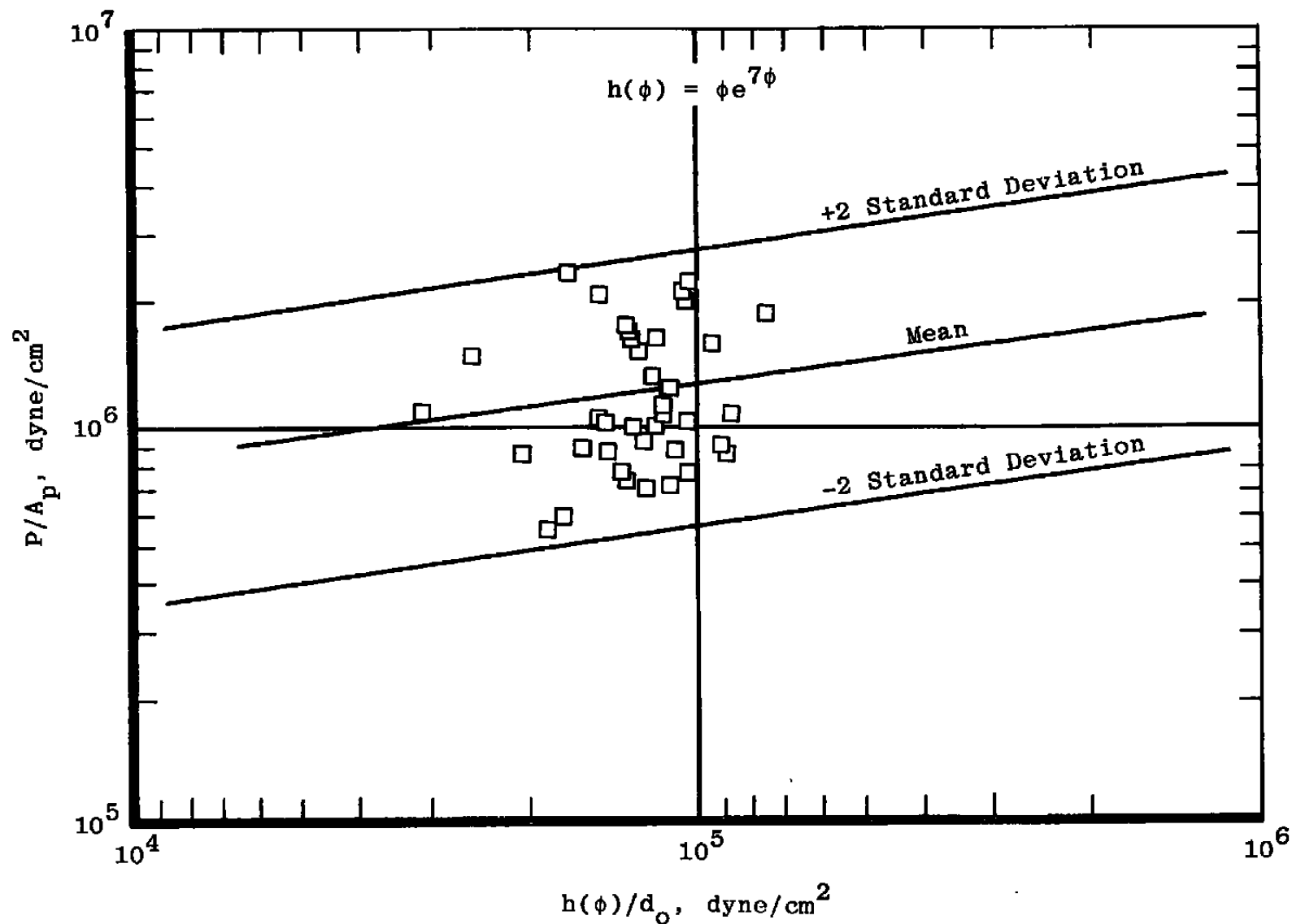


Figure 11. Crushing strength of aluminum oxide agglomerates.

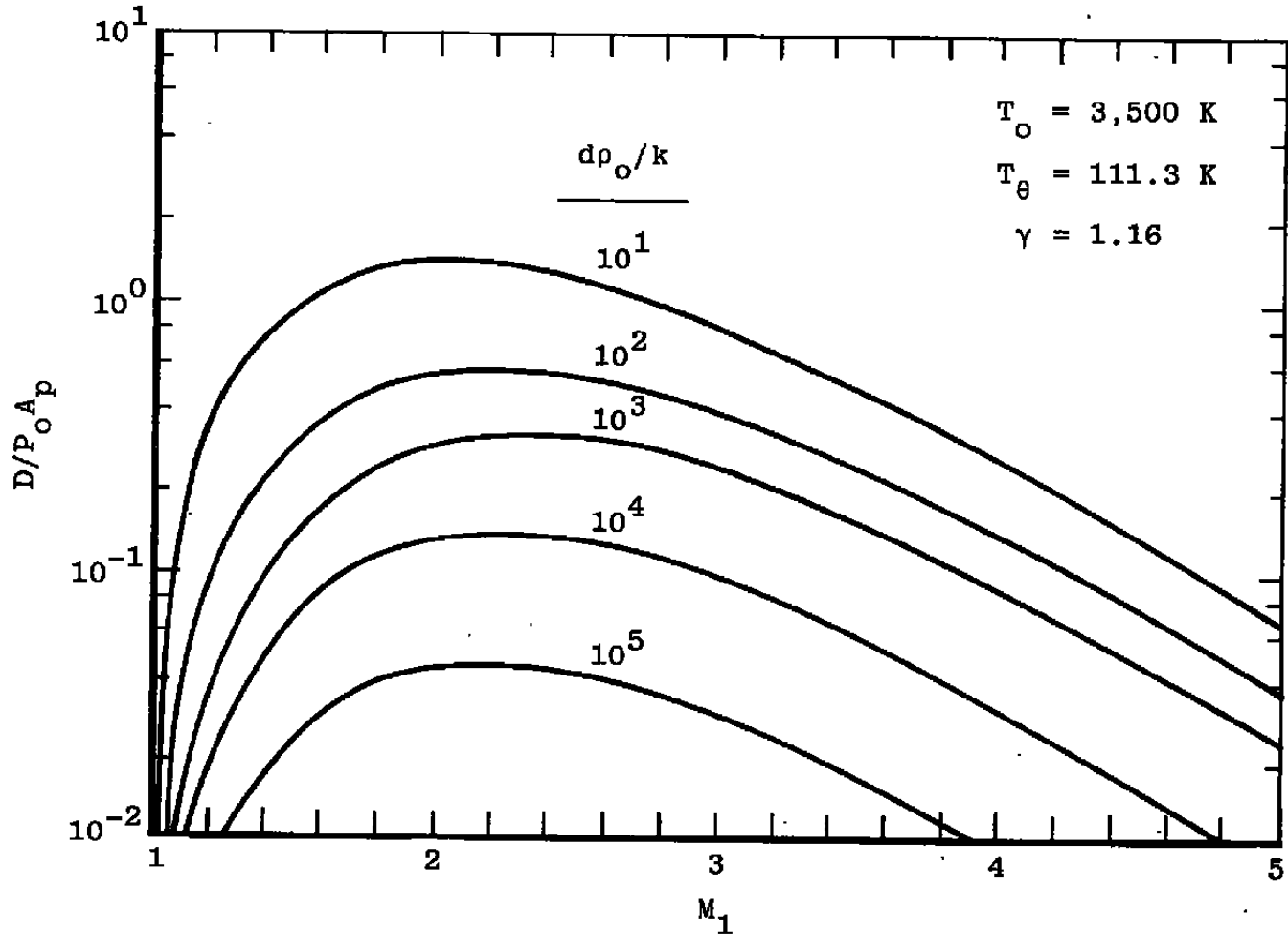


Figure 12. Normalized agglomerate drag.

**Table 1. Interparticle Bonding Forces**

Force of Adhesion	Particle Types Affected	Interparticle Force Equation	Typical Constant Values	Maximum Expected Force*
van der Waals	Clean, Dry, Uncharged Particles			
(a) London-Heitler		$F_{v1} = \frac{B1 d_0}{a^2}, a < 2,000 \text{ \AA}$	$B1 = 10^{-12} \text{ erg}$	$F_{v1} = 8 \times 10^{-3} \text{ dyne},$ $a = 10 \text{ \AA}$
(b) Lifshitz		$F_{v2} = \frac{B2 d_0}{a^3}, a > 2,000 \text{ \AA}$	$B2 = 10^{-20} \text{ erg-cm}$	$F_{v2} = 1 \times 10^{-10} \text{ dyne},$ $a = 2,000 \text{ \AA}$
Electrostatic	Particles Charged During Formation or Exposed to Ionized Gas	$F_e = \frac{\epsilon \pi d_0^2 q^2}{a^2}$	$\epsilon = 9 \times 10^{18} \text{ dyne-cm/coulomb}$	$F_e = 1.5 \times 10^{-2} \text{ dyne},$ 20 electron charge, $a = 10 \text{ \AA}$
Surface Film	Particles in a Condensable Vapor	$F_s = 2.2 \sigma_w d_0$	$\sigma_w = 72 \text{ dyne/cm}$ Water at Standard Conditions	$F_s = 1.3 \times 10^{-2} \text{ dyne}$

\* Calculations for a Unit Particle Size of  $0.8 \mu\text{m}$

**Table 2. Powders Used in Agglomeration Experiments**

Type	Manufacturer	Experimental Designation	Size Range, $\mu\text{m}$	Chemical Analysis <sup>(a)</sup> , percent	Agglomeration Achieved
$\text{Al}_2\text{O}_3$	Buehler	B-0.05	0.05	99.9 Al	No
$\text{Al}_2\text{O}_3$	Buehler	B-0.3	0.3	99.9 Al	No
$\text{Al}_2\text{O}_3$	Buehler	B-1.0	1.0	99.9 Al	No
$\text{Al}_2\text{O}_3$	Micro-Abrasives	M-1-99	1.0	99.4 Al 0.5 Si	Yes
$\text{Al}_2\text{O}_3$	Micro-Abrasives	M-1-97	1.0	97.0 Al 0.2 Si 0.5 Mg	Yes
$\text{Al}_2\text{O}_3$	(b)	RE	60 percent < 1  35 percent 1 to 3	86.0 Al 9.0 Fe  1.5 Ca 2.5 Cl	Yes
$\text{CaCO}_3$	(c)	C	1.0	99.9 Ca	No

<sup>(a)</sup>Analysis was performed using a Scanning Electron Microscope.

Indicated elements are metals or metal compounds.

<sup>(b)</sup>Material was collected in sludge pit after rocket motor tests.

<sup>(c)</sup>Commercially Available Ground Limestone

**Table 3. Estimated Measurement Errors**

Measurement Variable	Possible Causes for Error	Maximum Estimated Error
$d_o$ , $\mu\text{m}$	Monodisperse Powder Assumption	$\pm 0.4 \mu\text{m}$
$d$ , mm	Measurement Uncertainty of Microscope	$\pm 0.025 \text{ mm}$
$m$ , mg	Measurement Uncertainty of Microbalance	$\pm 0.050 \text{ mg}$
$P$ ; dyne	Nonvertical Loading	600 dyne
	Graduated Burret Reading	200 dyne
	Water Remaining in Loading Cylinder between Tests	100 dyne
	Variations in Water Density	50 dyne
	Variations in tare because of Agglomerate Placement	10 dyne

## APPENDIX A

### MEASUREMENT ERROR ESTIMATION PROCESS

Table 3 lists the measured parameters of these experiments, an associated list of possible factors affecting the measurement, and the maximum estimated error attributed to these factors. These error estimates were determined in the following manner.

The  $\pm 0.4\text{-}\mu\text{m}$  error in  $d_0$  was estimated from measurements of unit particle size in the SEM photographs. An average of  $0.8\text{ }\mu\text{m}$  was used as a constant value for  $d_0$ . The estimated errors in agglomerate diameter,  $d$ , and agglomerate weight,  $m$ , are those reported by the manufacturers of the microscope and the microscale, respectively.

The agglomerate crushing force parameter,  $P$ , has several factors affecting the measurement accuracy. The largest estimated error was caused by nonvertical loading applied to the agglomerate. The loading cylinder and slide moved in an arc about the hinged end of the 1.5-in. long slide. This error was reduced by mounting the loading cylinder at a 3-deg off-vertical angle towards the unhinged end of the slide. For the size range of agglomerates tested, the maximum error attributable to nonvertical loading was 600 dyne (approximately 0.04 percent).

The buret used to measure the amount of water added to the loading cylinder was graduated in 0.2-ml increments. Although readings were recorded to the nearest 0.1 ml, an estimated error of 0.2 ml (200 dyne) is listed, since additional water would always leave the buret in the time interval between agglomerate failure and buret stopcock closure. Another source of error was the initial cylinder between crushing experiments.

Finally, two small contributions to error in the crushing force measurement could be caused by variations in tap water density and initial agglomerate placement on the support base. The ideal value of water density was used in the calculations and was uncorrected for temperature or impurities. A maximum error of 50 dyne was arbitrarily estimated. Tare calculations were based on point-loading and exact-distance assumptions. Moving the agglomerate to various locations under the loading slide would theoretically change the required crushing force. During these experiments, however, careful attempts were made to place the agglomerate in the same location repeatedly, and the estimated error in Table 3 is representative of worse-case calculations based on experimental procedure.

# **NOMENCLATURE**

<b><math>A_p</math></b>	Agglomerate cross-sectional area, $\text{mm}^2$ , $= \pi d^2/400$
<b><math>a</math></b>	Particle separation distance, $\text{\AA}$
<b><math>B_1, B_2</math></b>	Constants in London-van der Waals equations, erg, erg-cm
<b><math>D</math></b>	Agglomerate drag behind shock, dyne
<b><math>d</math></b>	Agglomerate diameter, mm
<b><math>d_0</math></b>	Unit particle diameter, $\mu\text{m}$
<b><math>F</math></b>	Particle bonding force function, dyne
<b><math>F_e</math></b>	Electrostatic bonding force, dyne
<b><math>F_s</math></b>	Surface-film bonding force, dyne
<b><math>F_{v1}</math></b>	van der Waals bonding force, $a < 2,000 \text{\AA}$ , dyne
<b><math>F_{v2}</math></b>	van der Waals bonding force, $a > 2,000 \text{\AA}$ , dyne
<b><math>k</math></b>	Constant in Knudsen number function, $\text{gm}/\text{cm}^2$
<b><math>L</math></b>	Sample probe diameter, cm
<b><math>M_1</math></b>	Free-stream Mach number
<b><math>m</math></b>	Mass of agglomerate, gm
<b><math>P</math></b>	Agglomerate force of adhesion, dyne
<b><math>P_0</math></b>	Stagnation gas pressure, $\text{dyne}/\text{cm}^2$
<b><math>q</math></b>	Surface charge density, $\text{coulomb}/\text{cm}^2$
<b><math>R</math></b>	Universal gas constant, $\text{cm}^3\text{-atm}/\text{gmole-K}$

$T_o$	Stagnation gas temperature, K
$T_\theta$	Sutherland's constant, K, = 111.3 K for air
$W_b$	Particle Weber number
$Z$	Coordination number
$\gamma$	Gas specific-heat ratio
$\delta$	Bow shock detachment distance
$\epsilon$	Coulomb's law constant, dyne - cm <sup>2</sup> /coulomb
$\rho_a$	Agglomerate solids density, = mass/volume, gm/cm <sup>3</sup>
$\rho_o$	Stagnation gas density, gm/cm <sup>3</sup>
$\rho_p$	Density of aluminum oxide powder, = 3.7, gm/cm <sup>3</sup>
$\sigma$	Standard deviation
$\sigma_w$	Surface tension of water, dyne/cm